Thermographic Analysis of Thermo-mechanical Couplings

André Chrysochoos, Faycal Belmahjoub

Thermographic analysis of thermomechanical couplings

A. CHRYSOCHOOS and F. BELMAHJOUB (MONTPELLIER)

AFTER RECALLING the energy balance form in the case of elastic-plastic material, the relationships between the dissipation, stored energy of cold work and state variables were reviewed. An experimental set-up using an infra-red camera was introduced which enables us to establish continuous energy balance during uniaxial excitations. Mechanical tests were made at room temperature with four different materials (duraluminium, brass, carbon and stainless steels) under several uniaxial loading paths (tension, compression, loading-unloading and cyclic loading). Only the tests on duraluminium will be graphically shown in this paper, but results concerning the other materials will be mentioned. In particular, we shall show the energetical behaviour of materials immediately after deformation (time rate independence), during (elastic) unloading and during reversed straining.

1. Introduction

THE AIMS of this paper are the following.

First, a new and improved version of an infra-red device associated with a testing machine with numerical commands is presented. This experimental arrangement means that the energy balance in the case of uniaxial excitations at room temperature can be continuously determined during deformation test. The improvements, in comparison with previous apparatus [1 to 5], come essentially from technical progress in storing, processing and visualization of data given by the infra-red camera. This automatic data processing gives the experimentalist both greater accuracy in the measurements of the amounts of heat produced during deformation processes, and a greater flexibility in use.

Secondly, energy balances made on elastic-plastic materials under several mechanical quasi-static excitations are shown. In particular, the evolution of the stored energy after deformation during elastic unloading or reversed straining are presented and discussed in comparison with predictions of thermoelastoplastic models developed by [6] within the framework of the Generalized Standard Materials theory (G.S.M. theory [7 to 9]).

The energy balance form and the relationships between stored energy, dissipation and internal state variables are recalled in Sec. 2. The experimental arrangement and calibration procedure are presented in Sec. 3. Some experimental results concerning the dissipated and stored energy evolution are shown and compared with the numerical solutions obtained by computation of thermomechanical behaviour laws in Sec. 4. General concluding comments are given in Sec. 5.

2. Energy balance form

2.1. Mechanical aspects

In [10, 11] we have shown that, in the case of homogeneous and uniaxial excitations where the elastic deformation remains small, most classical kinematical approaches [12 to 16] lead to an additive decomposition of the strain rate tensor where the elastic and plastic parts can be measured without any doubt. A classical homogeneous test would

lead to

$$\dot{\varepsilon} = \dot{\varepsilon}_e + \dot{\varepsilon}_p. \tag{2.1}$$

Then, the volumic energy rate given hy the testing machine for a quasi-static deformation process (ignoring the kinetic energy) can be decomposed into

$$\dot{w}_{\text{ext}} = \sigma : \dot{\varepsilon} = \sigma : \dot{\varepsilon}_e + \sigma : \dot{\varepsilon}_p. \tag{2.2}$$

We shall call $\dot{w}_e$ the rate of volumic elastic energy, and $\dot{w}_a$ — the rate of volumic inelastic energy. The integration of Eq. (2.2) leads to

$$w_{\text{ext}} = w_e + w_a. \tag{2.3}$$

2.2. Thermodynamical aspects

Classical results of Thermodynamics of Irreversible Processes are used [17 to 20]. An homogeneous volume element of the sample is characterized by a set of $n + 1$ state variables. Let us take $T = \alpha_0$ as the absolute temperature, $\varepsilon_e = \alpha_1$ as the elastic strain, and $(\alpha_j)_{2\leq j\leq n}$ as the set of n 1 variables describing the hardening state. The volumic Helmholtz free energy is classically decomposed in [9]:

$$\psi(T, \varepsilon_e, \alpha_j) = \psi_e(T, \varepsilon_e) + \psi_s(T, \alpha_j)_{2\leq j\leq n}. \tag{2.4}$$

The "elastic" part of the free energy is due to the thermoelastic (reversible) part of the transformation. Supposing that the thermoelastic behaviour remains linear and isotropic [9 p. 140],

$$\psi_e = \left[\frac{1}{2}(\lambda\varepsilon_{e\text{I}} + 4\mu\varepsilon_{e\text{II}}) - (3\lambda + +2\mu)\lambda_{\text{th}}(T - T_0)\varepsilon_{e\text{I}}\right] - \frac{C_\alpha}{2T_0}(T - T_0)^2. \tag{2.5}$$

The second term is due to the strain hardening. During our quasi-static tests, the temperature variations remain small (around 0.5°C for elastic test and 5°C for cyclic elastoplastic test). In the vicinity of thermal equilibrium, these temperature variations are not taken into account.

$$\psi_s(T, \alpha_j)_{2\leq j\leq n} \simeq \psi_s(\alpha_j)_{2\leq j\leq n}. \tag{2.6}$$

In such conditions it has been shown [11] that internal energy variations associated with the hardening (stored energy of cold work) corresponds to free energy variation. It leads to the assumption that the (small) temperature variations induced by deformation do not modify the hardening state.

The 2nd Principle of Thermodynamics leads to the inequality of Clausius–Duhem:

$$\sigma : \dot{\varepsilon} - \frac{\partial\psi}{\partial\alpha_j}\dot{\alpha}_j - \frac{q}{T}\,\text{grad}(T) > 0, \quad 1 < j \leq n. \tag{2.7}$$

The intrinsic dissipation can thus be defined.

$$\mathcal{D}_1 = \sigma : \dot{\varepsilon}_p - \frac{\partial\psi_s}{\partial\alpha_j}\dot{\alpha}_j, \quad 2 \leq j \leq n. \tag{2.8}$$

Then, the rate of inelastic energy can be interpreted as the sum of two terms; Eqs. (2.2) to (2.8) lead to

$$\dot{w}_a = \sigma : \dot{\varepsilon}_p = \mathcal{D}_1 + \dot{\psi}_s. \tag{2.9}$$

If we denote by w_d the volumic amount of heat associated with the intrinsic dissipation, and by w_s—the stored energy of cold work per unit volume of sample, then

$$w_a = w_d + w_s. \tag{2.10}$$

The heat conduction equation is written as [11]

$$\rho C_\alpha \dot{T} - \operatorname{div}(k \operatorname{grad}(T)) = \rho \dot{w}_d - \rho T \frac{\partial^2 \psi}{\partial T \partial \alpha_j} \dot{\alpha}_j + r, \quad 1 \leq j \leq n. \tag{2.11}$$

The cross-terms at the r.h.s. can be eliminated for $j \geq 2$ because of Eq. (2.6). The first cross-term for $\alpha_1 = \varepsilon_e$ will be called the isentropic term $\rho \dot{w}_{is}$ associated with thermo-elastic effects. It is written with the aid of Eq. (2.5) as

$$\dot{w}_{is} = T \frac{\partial^2 \psi_e}{\partial T \partial \varepsilon_e} \dot{\varepsilon}_e = \lambda_{\text{th}} T_0 \operatorname{tr}(\dot{\sigma}). \tag{2.12}$$

Let us suppose that the external heat supply is time-independent, the heat conduction coefficient k, the linear thermal expansion coefficient λ_{th} and the specific heat C_α are assumed to be independent of the hardening state.

Then, if we denote $\theta = T - T_0$, the heat conduction equation can be simplified to the form

$$\rho C_\alpha \dot{\theta} - k \Delta \theta = \rho(\dot{w}_d - \dot{w}_{is}).$$

The mechanical heat source will be denoted $\dot{w}_{ch}$,

$$w_{ch} = w_d - w_{is}. \tag{2.14}$$

The energy balance form can be summed up in Eqs. (2.3), (2.10) and (2.14). The last quantity which may be introduced and associated with the energy balance is the stored energy ratio defined as

$$F = \frac{w_s}{w_a} \times 100. \tag{2.15}$$

3. Experimental set-up and calibrations

3.1. General description

The experimental set-up essentially consists of a 100 kN Screw Machine and an Infra-red Camera. The Testing Machine is made and commercialized by DARTEC Society (England). Tests and machine (*1*, *2*) are driven by micro-computer (*3*), (Cf. Sketch 1).

The Infra-red Camera is built and commercialized by AGENA Infra-red Systems (Sweden). This device is equipped with the digitization system initially conceived by J. C. Chezeaux and B. Nayroles (France) [1-4] which was then developed and improved by the authors. A second micro-computer drives the data storing, and processing, and provides the visualization of the "thermal scenes". The camera (*7*) (Cf. Sketch 2) is placed directly on the crosshead (*1*) of the Testing Machine. The thermoregulation is carried out carefully. The test area must be completely closed. The air is circulated by electric fans and the room temperature is kept constant by means of two heat sources. The video signal quality is improved by anti-radiation screens (*4*) in order to intercept parasitic reflections coming from the surroundings.

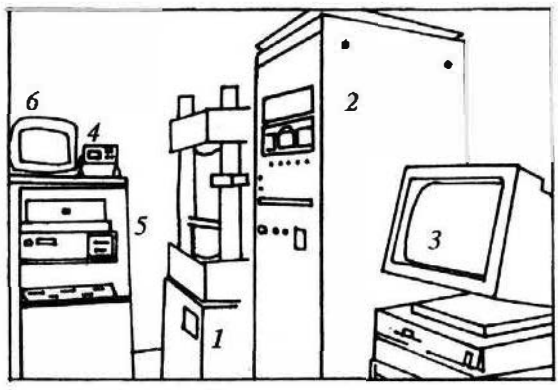

SKETCH 1. Basic sketch of the testing room: *1*—100 kN screw machine, *2*—command unit, *3* microcomputer driving the testing machine, *4* infra red camera display unit, *5*—digitization system of the video signal, *6* micro-computer for infra-red data recording, processing and visualization.

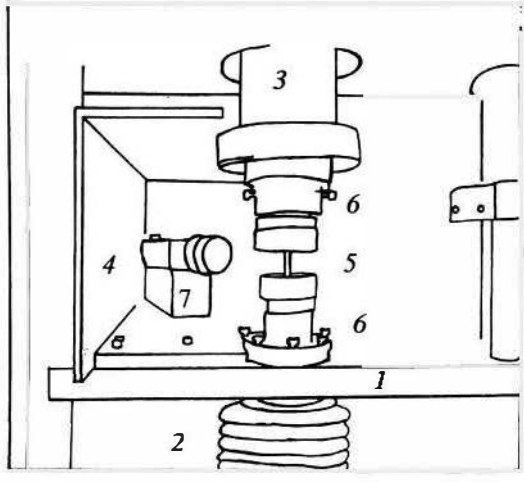

SKETCH 2. Basing sketch of the experimental set up: *1* moving crosshead, *2* screw jack, *3*—load cell, *4* anti radiation screens. *5*—sample, *6*—grips, *7*—I.R. camera.

3.2. Digitized thermal pictures

They are matrices of 256 lines per 180 columns digitized on 12 bits. The digitization system allows for recording, at the beginning of each line, both signals as "thermal level" and "thermal range" characterizing the state of the camera, and six electrical signals through two-stage amplifiers, such as load and deformation signals, room temperature, etc. In our case, (with optional 20° fixed front lens), the spatial resolution is $d_x = (270 \pm 10) \cdot 10^{-6}$ m and $d_z = (180 \pm 5) \cdot 10^{-6}$ m. The sensitivity in temperature variation is around $5 \cdot 10^{-3}$ °C in the vicinity of room temperature (25°C). In Fig. 1 a thermal map of a stainless steel (A304) is shown. These results are taken from a cyclic test.

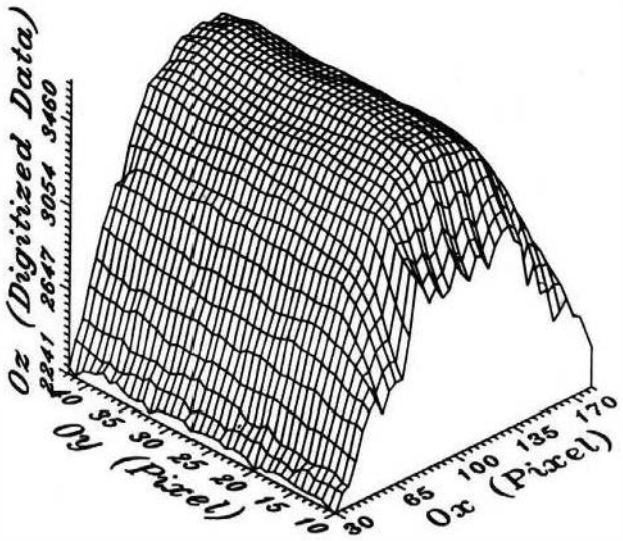

FIG. 1. Digitized thermal map; the spatial resolution is $d_x = 270\mu m$ and $d_x = 180\mu m$. The sensitivity is around 130 digit $°C^{-1}$.

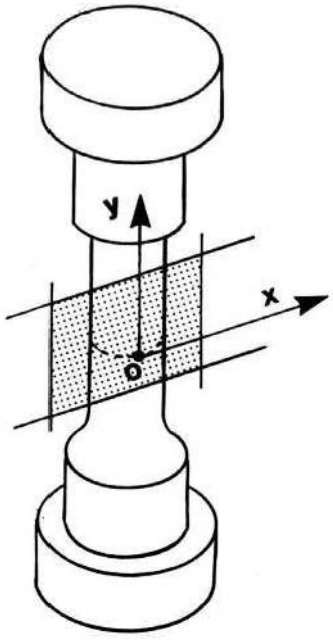

FIG. 2. Definition of the "temperature of the sample".

During a mechanical test, the material points of the sample move within the frame of reference of the camera. Knowing the displacement field at each time t in the case of homogeneous and uniaxial excitations, one can thus determine the correspondence between material points and pixels. The computer uses the information given by the extensometer stored at the beginning of each line of thermal pictures to establish this correspondence automatically. We shall define in the following sections and sub-sections "the temperature of a sample" as that of the material point which is placed at the middle point of one generatrix of the cylindrical sample (Cf. Fig. 2).

3.3. Calibration of the video signal

A special warming target was made to calibrate the variations in video signal in the vicinity of 25° C (Cf [6] for technical details). The response of the infra-red detector (MCT detector, liquid nitrogen cooled) was strongly nonlinear even in the vicinity of thermal equilibrium. The calibration law was approximated to the following quadratic law

$$T_{th} - T_0 = a(s_c - s_0)^2 + b(s_c - s_0), \tag{3.1}$$

where a and b are constants.

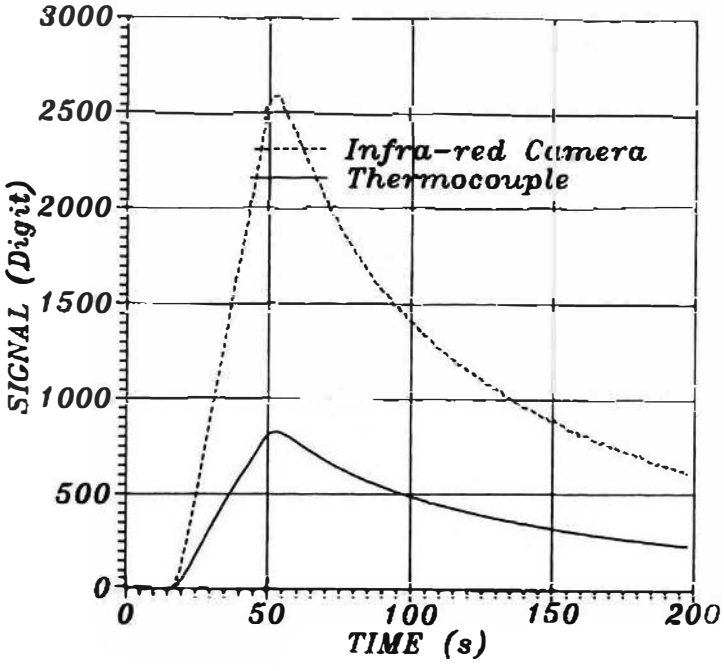

FIG. 3. Dynamic calibration of the video signal.

The calibration can be performed in a dynamic way. It does not need to wait for thermal equilibrium and thus can be done frequently. A calibration test is shown in Fig. 3.

3.4. Calibration of thermal losses

In the heat conduction equation (2.13), the Laplacian of temperature can be seen. From an experimental point of view this term is quite difficult to evaluate directly for good thermal conductors like aluminium or copper alloys, and even for steels in the vicinity of thermal equilibrium with small thermal gradients. A phenomenological hypothesis is used to determine the volumic losses $k/(\rho C_\alpha)\Delta\theta$. We shall suppose that in the vicinity of thermal equilibrium, the radial heat flows by radiation and convection in the air, and the axial heat losses by conduction in the sample, are well modelled by linear temperature laws. This hypothesis leads to [5]

$$\frac{k}{\rho C_\alpha}\Delta\theta \cong \frac{\theta}{\tau_{th}}, \tag{3.2}$$

where τ_{th} is a time constant characterizing the losses. The validity of this important hypothesis is checked using thermoelastic effects. In Fig. 4, thermal evolution calculated with Eqs. (2.12), (2.13) and (3.2), for the case of cyclic excitation on duraluminium is compared with experimental evolution. In this figure the temperature is averaged over a small surface of 2×2 mm^2 in order to improve the signal-to-noise ratio. This kind of control was done on each studied material before the new experiment. In the case of duraluminium, the following value of τ_{th} was used:

$$\tau_{th} = 3.6 \text{ s}.$$

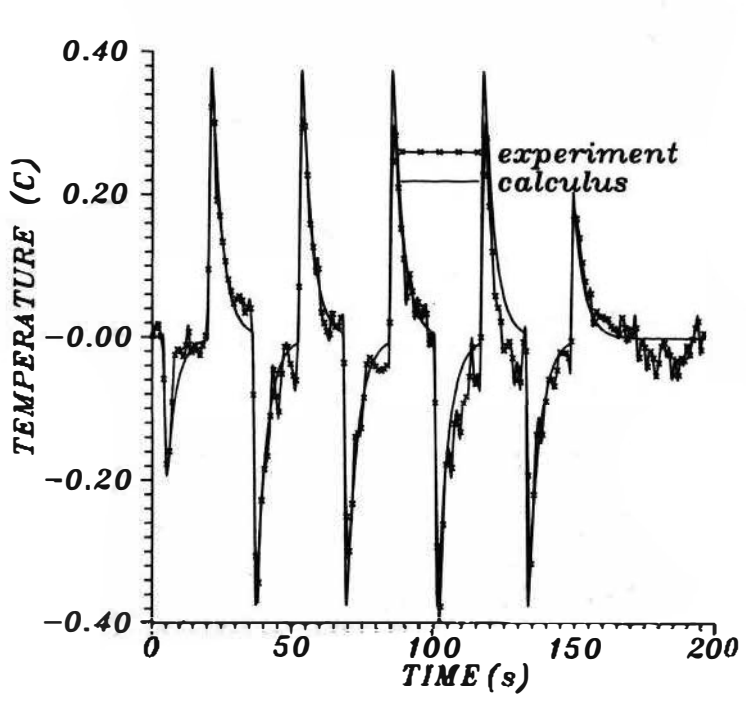

FIG. 4. Thermoelastic effects; comparison of the experimental temperature evolution with the theoretical one. Calibration of the thermal losses.

This constant depends on the geometrical form of the sample, the type of material, and the point and its vicinity observed by the camera.

4. Results

4.1. GSM models

To predict the mechanical behaviour of the studied material the Generalized Standard Material Theory was used. The models gave results being in good agreement with mechanical experiments. They are presented in details in [6; p. 47–83]. They represent a superposition of classical and elementary models, such as isotropic hardening, linear and non linear kinematical hardening models. Once their mechanical identification is done, these models can predict the energy balance evolution.

4.2. Thermomechanical couplings

The observed and calculated temperature evolutions of duraluminium associated with a series of loading-unloading excitations are shown in Figs. 5 and 6, respectively. During the elastic unloading ($A - B$), the "experimental" temperature ($a - b$) remains approximately constant and the "theoretical" one decreases slowly. The stress rate, which is the same in both cases (around 30 MPa/s) generates a positive source during unloading (cf. Eq. (2.13)), and this one is, in this case, just sufficient for the thermal losses in the first case. This is not true for the "theoretical" temperature, which is higher.

During the elastic reloading ($B - A'$), the stress rate changes its sign and becomes more important (around 150 MPa/s): the sample cools along ($b - a'$) in both cases.

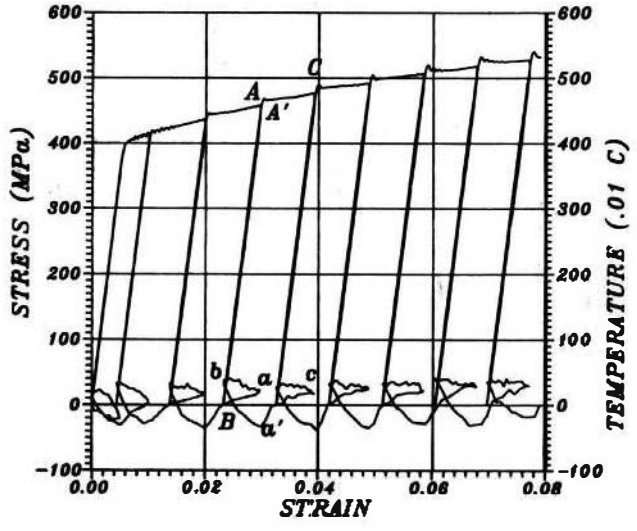

FIG. 5. Thermomechanical couplings on a duraluminium sample during a series of loading-unloading excitations. Experimental data.

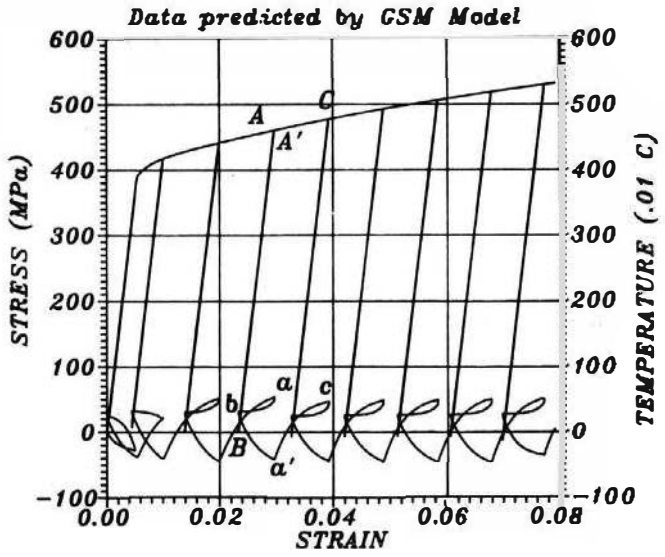

FIG 6. Thermomechanical couplings on a duraluminium sample during a series of loading-unloading excitations. Calculated data.

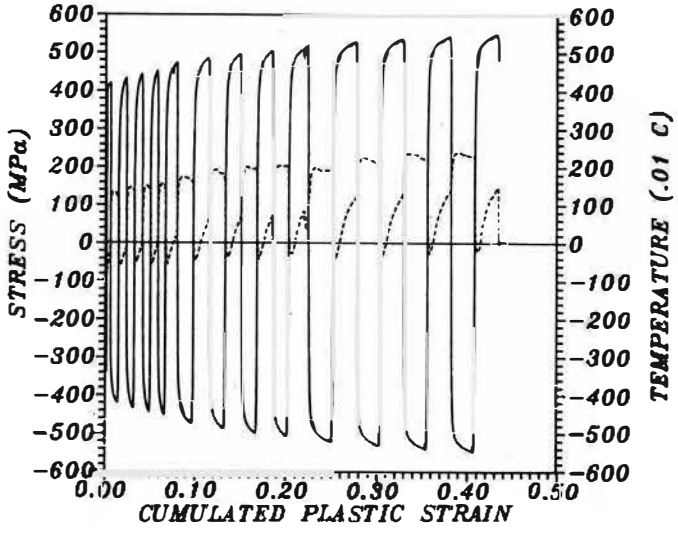

FIG. 7. Thermomechanical couplings on a duraluminium sample during cyclic straining. The strain limits are: ±0.5%, ±1.0%, ±1.5% and ±2.0%.

When the actual yield stress is reached, dissipative phenomena appear. These are generally more important than the thermoelastic effects: during (A' C) stress path, the sample warms again from a' to c.

A second example is illustrated by Fig. 7. The temperature evolution during cyclic straining is shown. The plastic strain rate is around 10^{-3} s^{-1}. Four stages of four cycles

were imposed with the following strain limits: ±0.5%, ±1.0%, ±1.5%, and ±2.0%. The first stage is difficult to see in Fig. 7 because the behaviour remains elastic during this stage and the curves are plotted versus the cumulated plastic strain. The dashes represent the temperature variations which reached approximately 2°C during the test. For the same kind of mechanical excitation, the carbon steel samples reached 4°C of temperature variations and the stainless steel samples, 10°C, [Cf. 6 p. 134–141].

4.3. Energy balances

Taking into account the data of Figs. 5 and 6, Figure 8 and 9 introduce the measured and the calculated energy balance evolutions, respectively.

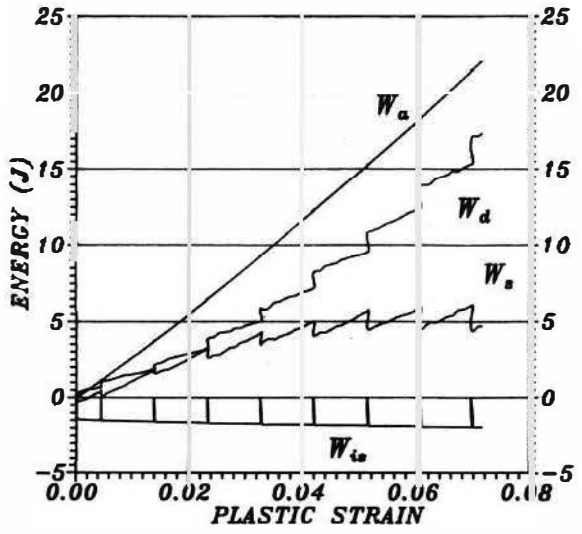

FIG. 8. Energy balance evolution of a duralumin sample during a series of loading unloading excitations. Experimental data: release of stored energy can be observed during elastic unloading.

First, we can observe differences between the amounts of stored energy determined by both approaches. The stored energy predicted by our model is less than that given by the experimental data analysis. This fact was observed for all the four studied materials.

Secondly, release of stored energy appears in Fig. 8, during elastic unloading. But the stored energy release leads to an evolution of the hardening state variables (cf. Eq. (2.8)) during an elastic deformation path, and that kind of phenomenon cannot be predicted by the Classical Theory of Elastoplasticity: in Fig. 9, naturally, no evolution of stored energy can be observed during elastic unloadings!

Experiments showed similar results during elastic unloading of brass samples but these releases were not observed in case of steel. Figures 10 to 12 must be associated with cyclic excitations illustrated by Fig. 7. Experimental energy balance evolution is plotted versus the cumulated plastic strain in Fig. 10. During reversed straining, small amounts of stored energy are dissipated. Experiments performed by [21] showed such phenomenon during tension-compression tests on copper samples. It can be predicted by Generalized

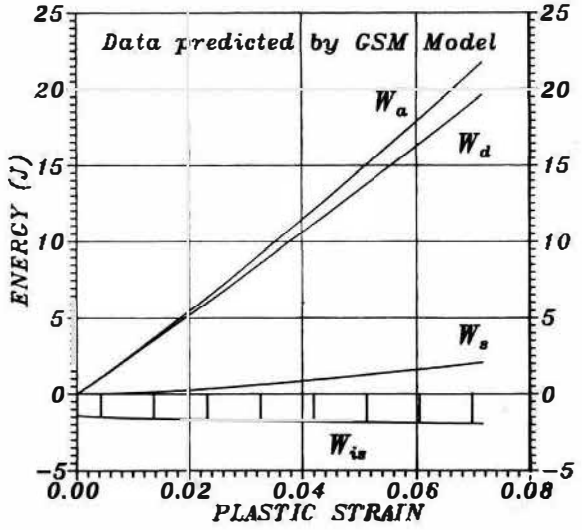

FIG. 9. Energy balance evolution of a duraluminium sample during a series of loading-unloading excitations. Calculated data: no release of stored energy can be predicted during elastic unloading with elastic plastic models.

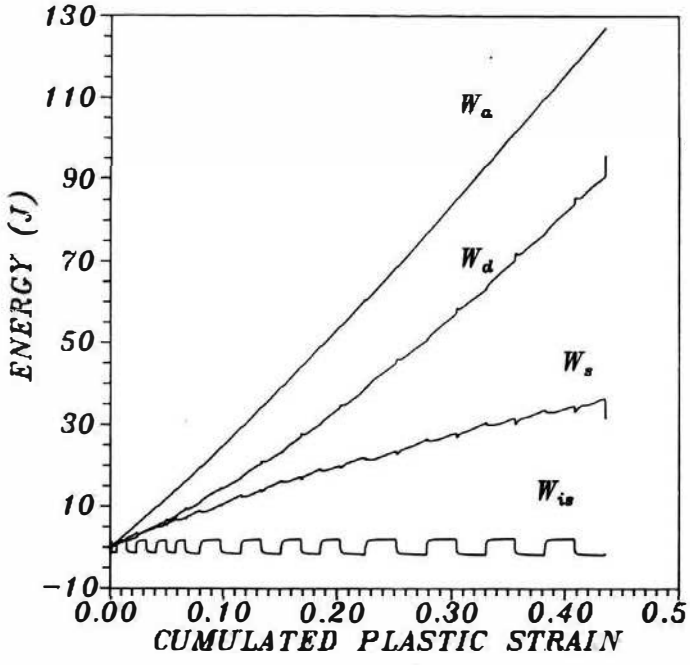

FIG. 10. Energy balance evolution of a duraluminium sample during cyclic excitations. Release of stored energy can be observed after deformation.

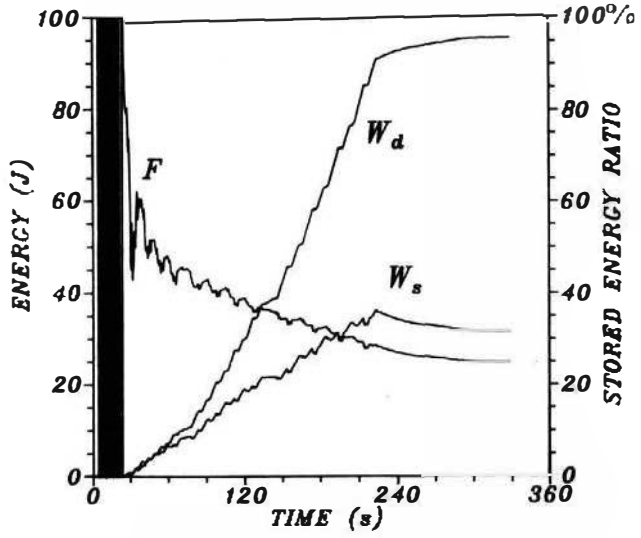

FIG. 11. Dissipated and stored energy evolutions during cyclic test on a duraluminium sample. Experimental data: the releases after deformation can be seen as a function of time. A general decrease of the stored energy ratio can be observed.

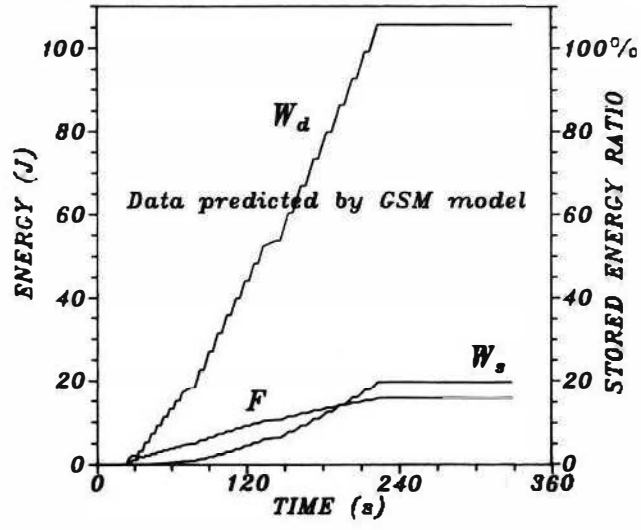

FIG. 12. Dissipated and stored energy evolutions during cyclic test on a duraluminium sample. Calculated data: no release after deformation can be predicted by time-rate independent models. A general increase of the stored energy ratio can be observed.

Standard Materials models as long as they take into account a nonlinear kinematical hardening [21 p. 213–239]. In this case, release appears just after straining reversal when the thermodynamical force X and the flux $\dot{\alpha}$ of the associated state variable have opposite

signs, and thus:

$$\dot{w}_s \cong X : \dot{\alpha} \leq 0. \tag{4.1}$$

The measured and the calculated, dissipated and stored energies have been plotted versus time in Fig. 11 and Fig. 12, respectively. Time has been chosen as X variable in order to point out in Fig. 11 the release of stored energy observed after deformation. This phenomenon has already been observed by [22, 23] on copper alloy samples. Naturally the time-rate independence supposed in the classical theory of elastoplasticity does not allow the models to predict this kind of release. Of course, one can observe that the calculated stored energy remains constant after deformation in Fig. 12.

The stored energy ratio can be seen at both graphs. At the beginning of the strain hardening, the stored energy ratio is difficult to evaluate because W_s and W_a tend theoretically to zero with cumulated plastic strain. That is the reason why numerical noise appears in Fig. 11. The initial stored energy ratio can be estimated at 50%. The same order of magnitude has been observed in experiments on brass and steels. Theoretically, the models will automatically predict an initial stored energy ratio equal zero provided that the initial values of the thermodynamical forces start from zero. This result is illustrated in Fig. 12.

5. Concluding remarks

We have tried to show in this paper the new technical performances of an experimental set-up able to perform continuous energy balance on a sample during quasi-static mechanical excitations. In comparison with the previous versions of the device, the data storing, processing and visualization have considerably improved. This progress gives greater flexibility of use and greater capability of the infra-red data interpretation and of establishing the energy balance.

Some experiments on duraluminium are presented. The first observation which can be made is that thermomechanical models drawn up within the framework of the classical theory of the time-rate independent elastoplasticity, are not automatically capable of predicting dissipation or stored energy evolution in agreement with experimental observations, even if they give correct mechanical predictions. For instance, releases of stored energy or heat evolved by dissipation were observed during elastic unloading (reversible path), or after deformation (time dependence).

Acknowledgements

This study was supported by the Centre National de la Recherche Scientifique and the Direction des Recherches Etudes et Techniques. In particular, the authors would like to thank Dr B. NAYROLES (CNRS) and J. P. GRELLIER (DRET) for their encouragements and J. C. CHEZEAUX for providing the digitization system of the IR camera.

References

1. B NAYROLES, R. BOUC, H. CAUMON, J. C. CHEZEAUX, E. GIACOMETTI, *Téléthermographie infra-rouge et mécanique des structures*, Int. J. of Eng. Sci., 19, pp. 929 947, 1981
2. P BREMOND, *Développement d'une instrumentation infra-rouge pour l'étude des structures mécaniques*, Th. I.D., LMA, CNRS, Marseille, 1982.

3. J. C. Chezeaux, *Un controleur d'acquisition numérique d'image thermique; interface caméra IR AGA 780, PDP 1164, PDP 1124*, Note Interne LMA, CNRS, Marseille, 21000, 1984.
4. R. Bouc, B. Nayroles, *Méthodes et résultats en thermographie IR des Solides*, J. de Mec. Theo. et Appl., **4**, 1985.
5. A. Chrysochoos, J. C. Chezeaux, H. Caumon, *Analyse thermomecanique des lois de comportement par thermographie infra rouge*, **24**, pp. 215 225, 1989.
6. F Belmahjoub, *Comportement thermomecanique de matériaux métalliques sous divers trajets de chargement uniaxés*, Th. Doctorat, Montpellier 1990.
7. B. Halphen, Q. S. Nguyen, *Sur les matériaux standards généralisés*, J. de Mec., **14**, 1, 1975.
8. P. Germain, Q. S. Nguyen, P. Suquet, *Continuum thermodynamics*, J. Appl. Mech., 105, 1983.
9. J. Lemaitre, J. L. Chaboche, *Mécanique des matériaux solides*, Dunod Ed., 1985.
10. A. Chrysochoos, *Dissipation et blocage d'énergie lors d'un écrouissage en traction simple*, Th. d'Etat, Montpellier 1987.
11. A. Chrysochoos, O. Maisonneuve, G. Martin, H. Caumon, J. C. Chezeaux, *Plastic and dissipated works and stored energy*, Nucl Eng. and Des., 114, pp. 323–333, 1989.
12. A. E. Green, P. M. Naghdi, *A general theory of elastic-plastic continuum*, Arch. Rat. Mech. Anal., 18, pp 259–281, 1964.
13. E. H. Lee, *Elastic-plastic deformation at finite strain*, J. Appl. Mech., **36**, pp. 1–6, 1969.
14. F. Sidoroff, *On the formulation of plasticity and viscoplasticity with internal variables*, Arch. Mech., **27**, 5–6, pp. 807–889, 1975.
15. S. Nemat Nasser, *Decomposition of strain measures . . .*, Int. J. of Solid Struct., **15**, pp. 155 166, 1979.
16. A. Chrysochoos, *Bilan énergétique en élastoplasticité grandes déformations*, J. de Mec. Théo. and Appl., **4**, 5, pp. 589–614, 1985.
17. L. Onsager, *Reciprocal relations in irreversible process*, Phys. Rev., **37**, 405, 1931.
18. C. Eckart, *Thermodynamics of irreversible processes*, Phy. Rev., **58**, 276, 1940.
19. M. Gurtin, *On thermodynamics of materials with memory*, Arch. Rat. Mech. Anal., **28**, 40, 1968.
20. J. Mandel, *Variables cachées, Puissances dissipée, dissipativité normale*, Sci. et Tech. de l'Armement, **54**, 4 Fasc., 1989.
21. G. R. Halford, *Stored energy of cold work changes by cyclic defomation*, Ph. D. Thesis, University of Illinois, Urbana, 1966.
22. R. O. Williams, *A deformation calorimeter*, Rev. Sci. Inst., **31**, 12, 1960.
23. R. O. Williams, *The stored energy of copper at 24°C*, Acta Met., **13**, 1965.

LABORATOIRE DE MECANIQUE GENERALE DES MILIEUX CONTINUS
UNIVERSITE MONTPELLIER II, MONTPELLIER, FRANCE.